

Kinetics of photodegradation and nanoparticle surface accumulation of a nanosilica/epoxy coating exposed to UV light

Hsiang-Chun Hsueh, Deborah S. Jacobs, Justin M. Gorham,
Savelas A. Rabb, Lee L. Yu, Chun-Chieh Tien, Tinh Nguyen, Lipiin Sung 

© American Coatings Association (outside the USA) 2017

Abstract Temperature effect on the kinetics of photodegradation and surface accumulation of nanoparticles in an epoxy nanocoating exposed to ultraviolet light (UV) was investigated. A model epoxy coating containing 5% untreated nanosilica was selected. Exposed film specimens were removed at specified UV dose intervals for measurements of chemical degradation of the epoxy component, and nanosilica accumulation on specimen surface release as a function of UV dose for four temperatures. The chemical degradation was measured using Fourier transform infrared spectroscopy, X-ray photoelectron spectroscopy, and UV–visible spectroscopy. Atomic force microscopy was employed to determine the kinetics of nanosilica accumulation on the nanocoating surface during UV exposure. The temperature dependence behaviors of kinetic parameters obtained by various measurement techniques will be used to better understand the degradation mechanism and surface accumulation of nanoparticles in exterior nanocoatings.

Keywords AFM, FTIR, Nanocoatings, Surface morphology, UV degradation, XPS

Introduction

Polymeric materials containing nanofillers (polymer nanocomposites) have attracted growing interest due to their outstanding properties as well as their unique applications.^{1,2} Polymer nanocoatings, a subclass of nanocomposites, are increasingly used outdoors such

as on building structures, airplanes, and automobiles, because of their excellent mechanical, gas barrier, self-cleaning, and UV resistance properties.^{3–7}

Studies have long indicated that most common polymers undergo significant degradation during exposures to outdoor environments.^{8–15} A serious consequence of the matrix degradation for nanocoatings is that the nanofillers embedded in the polymer matrices could be released via the effect of rain, snow, condensed water, and wind. Such nanoparticle release during nanocoating life cycle is a concern, because engineered nanofillers have been shown to be hazardous to the environment and human health.^{10,11,15–18}

Taking advantage of the highly uniform and high-intensity UV radiation from the SPHERE (Simulated Photodegradation via High Energy Radiant Exposure) device,¹⁹ the National Institute of Standards and Technology (NIST) has investigated the degradation rate, nanomaterial surface accumulation, and nanomaterial release for a model epoxy (without UV stabilizers) containing silica nanoparticles.^{20–24} In a previous study on an amine-cured epoxy nanocoating exposed to UV radiation at 60°C/≈ 0% relative humidity (RH) exposure condition, we have found that the epoxy matrix in the nanocoating underwent rapid photodegradation during exposure to 295 nm to 400 nm UV, exposing nanosilica on the surface and subsequently releasing it from the nanocoating.²³

Although nanosilica accumulated on the surface and subsequent release from the nanocoatings was observed and measured,²³ the role of temperature on the photodegradation rate, surface accumulation, and release of nanoparticles has not been investigated. Temperature is an important factor in the degradation process of polymers. In this study, we examined how temperature affects both the photodegradation of polymer matrix and surface accumulation of nanosilica during UV exposures of an epoxy nanocoating. The resulting knowledge of temperature dependence

H.-C. Hsueh, D. S. Jacobs, J. M. Gorham,
S. A. Rabb, L. L. Yu, C.-C. Tien, T. Nguyen,
L. Sung (✉)
National Institute of Standards and Technology,
Gaithersburg, MD, USA
e-mail: lipiin@nist.gov

behaviors on kinetic parameters obtained by different measurements will be useful for understanding the degradation mechanism and predicting the long-term release of nanoparticles in exterior nanocoatings.

Experimental procedures

Materials and preparation of nanocoating

Unless stated, the silica nanoparticles (i.e., nanosilica) were an untreated material in powder form, having a normal diameter of 15 nm and a purity greater than 99.5% (provided by manufacturer). The epoxy coating was a model stoichiometric mixture of a diglycidyl ether of bisphenol A (DGEBA) epoxy resin having an equivalent mass of 189 (grams of resin containing one gram equivalent of epoxide) and a tri-polyetheramine curing agent. There were no UV stabilizers added to the amine-cured epoxy coating. It should be noted that, due to steric hindrance and restricted transport during the late curing stages, some residual unreacted epoxide and amino groups are expected to be present in the coating films after curing. The presence of these functional groups and impurities (e.g., residual catalysts, processing aids) may have an influence on the photodegradation of an amine-cured epoxy coating. The solvent used for nanoparticle dispersion and coating processing was reagent grade toluene (purity > 99.5%). The chemical structures of the components and the cured epoxy coating are given elsewhere.²² Free-standing films having a thickness between 125 and 150 μm of the amine-cured epoxy containing 5% mass fraction of nanosilica were prepared following the procedure described in reference (21). All films were cured at ambient conditions (24°C and 50% RH) for 1 d, followed by post-curing for 45 min at 110°C in an air circulating oven. The quality of all epoxy/nanosilica coating (epoxy nanocoating) films was assessed by visual inspection for evidence of air bubbles or defects (cracks). Specimens were only selected from defect-free regions.

UV exposure

Specimens of epoxy nanocoating were exposed to <1% RH at four different temperatures, 30, 40, 50, and 60°C in the NIST SPHERE UV chamber.²⁰ The very dry condition was used to minimize any effect of water on the photodegradation of epoxy. The NIST SPHERE UV chamber produces a highly uniform UV flux of approximately 140 W/m^2 in the wavelength range of 295–400 nm. The equivalent accelerating factor of SPHERE exposure is estimated to be 15x compared with the typical outdoor exposures in Florida with an estimated dosage of 285 MJ/m^2 per year for the wavelengths between 295 and 385 nm.²⁵ Specimens for characterizing surface morphology had a dimension

of 10 mm \times 10 mm, and those for tracking chemical changes had a diameter of 19 mm. Specimens were removed after specified accumulated UV doses (i.e., at specified time intervals) for various characterizations. UV dose, in MJ/m^2 , is defined here as the total accumulated energy resulting from repeated UV radiation exposures at a particular time period per unit irradiated surface. Because the SPHERE was operated without interruption during this experiment, its UV dose is linearly proportional to exposure time.

Characterization of nanocoating degradation and surface morphological changes

The chemical degradation of both neat epoxy and nanocoating was measured using molecular spectroscopy via attenuated total reflection Fourier transform infrared spectroscopy (ATR-FTIR), X-ray photoelectron spectroscopy (XPS), and UV–visible spectroscopy (UV–Vis). ATR-FTIR spectra were recorded at a resolution of 4 cm^{-1} using dry air as a purge gas and a spectrometer (Nexus 670, Thermo Nicolet) equipped with a liquid nitrogen-cooled mercury cadmium telluride (MCT) detector. A ZnSe prism and 45° incident angle were used for the ATR-FTIR measurement. All spectra were the average of 128 scans. The peak height was used to represent the infrared intensity, which is expressed in absorbance, *A*. All FTIR results were the average of four specimens. UV–visible spectra were recorded using an HP 8452A spectrometer fitted with an autosampler. Spectra were collected for wavelengths from 190 to 1100 nm with an integration time of 0.5 s.

XPS was used for elemental and chemical state analysis of the nanocoatings. Analyses were carried out using an Axis Ultra DLD spectrophotometer (Kratos Analytical) equipped with a monochromated Al $K\alpha$ X-ray source (1486.6 eV). The photoelectrons were collected along the surface normal at a pass energy 40 eV and a step size of 0.1 eV/step for the C(1s), Si(2p), O(1s), and N(1s) regions. All XPS spectra were fit with a Shirley baseline and adjusted with the appropriate elemental sensitivity factors to obtain information on percent composition.

Surface morphological changes of nanocoating were followed by tapping mode atomic force microscopy (AFM) at ambient conditions (24°C, 50% RH) using a Dimension Icon system (Bruker, USA) and silicon probes (TESP, Bruker). Both topographic (height) and phase images were obtained simultaneously using a resonance frequency of approximately 300 kHz for the probe oscillation and a free-oscillation amplitude of 62 $\text{nm} \pm 2 \text{ nm}$. Height images of a scan size of 20 μm were analyzed by the image software provided by the AFM instrument, and the function of bearing analysis was used to follow the nanosilica accumulation on the nanocoating surface with UV exposure. The results are the average of three different locations.

Results

Surface morphological changes

Figure 1 displays AFM height and phase images of unexposed and UV-exposed epoxy nanocoating surface at, as an example, 40°C. Contrast in the height images of Fig. 1a is due to the surface topography, with little evidence of nanoscale particles being present on the surface, which is also confirmed in the featureless phase image (Fig. 1a, right). As the UV dose increased, the surface roughness increased and nanoparticles or clusters of nanoparticles appeared on the surface, as shown in both the height and phase images of Fig. 1b. Brightness of the particles in the height image indicates that they were near and above the surface. The phase image also shows a strong contrast between the nanoparticles and the matrix, which is typically observed for mixtures of a high modulus inorganic material and a low modulus polymeric material.

Figure 2 shows the surface morphological changes of the nanocoating exposed to different UV doses in four temperatures (30, 40, 50, and 60°C). All four temperatures showed similar effects. The number of particles on the surface increased with increasing UV dose, and the size of the particle clusters and the number of connected clusters also increased with UV dose. After 400 MJ/m² dose, a layer of compact particles almost covered the entire surface for all four

temperatures. Similar results were observed in NIST previous studies for a silane-treated nanosilica in a similar epoxy system.^{20,22}

To follow the accumulation of nanosilica on the nanocoating surface during UV exposure, an AFM software image analysis was conducted on height images. Figure 3 displays the surface coverage (in %) of revealed particles (assuming as nanosilica clusters) as a function of UV dose. The offset of 20% particle coverage is due to the initial rough nanocoating surface, which resulted in an overestimation of the surface coverage of the larger particle clusters. The rough surface morphology as observed in the raw AFM height image (Fig. 1a) may affect the gray-level threshold (flatness in the bearing analysis function) and consequently the percentage value of the peaks (white dots).

It shows that the accumulation of nanosilica on the UV-exposed nanocoating increased rapidly between 0 and 300 MJ/m² dose but slowed down substantially thereafter. The dose amount of 300 MJ/m² of UV is roughly what is seen in a harsh outdoor environment such as Florida or Arizona per year.^{25,26} The shape of nanosilica coverage vs UV dose curve is similar to the chemical changes such as oxidation measured by FTIR with UV dose,²³ suggesting that the accumulation of nanosilica on the nanocoating surface with UV exposure is closely related to photodegradation of the epoxy matrix; that is, as the epoxy layer on the nanocoating surface was degraded by UV radiation,

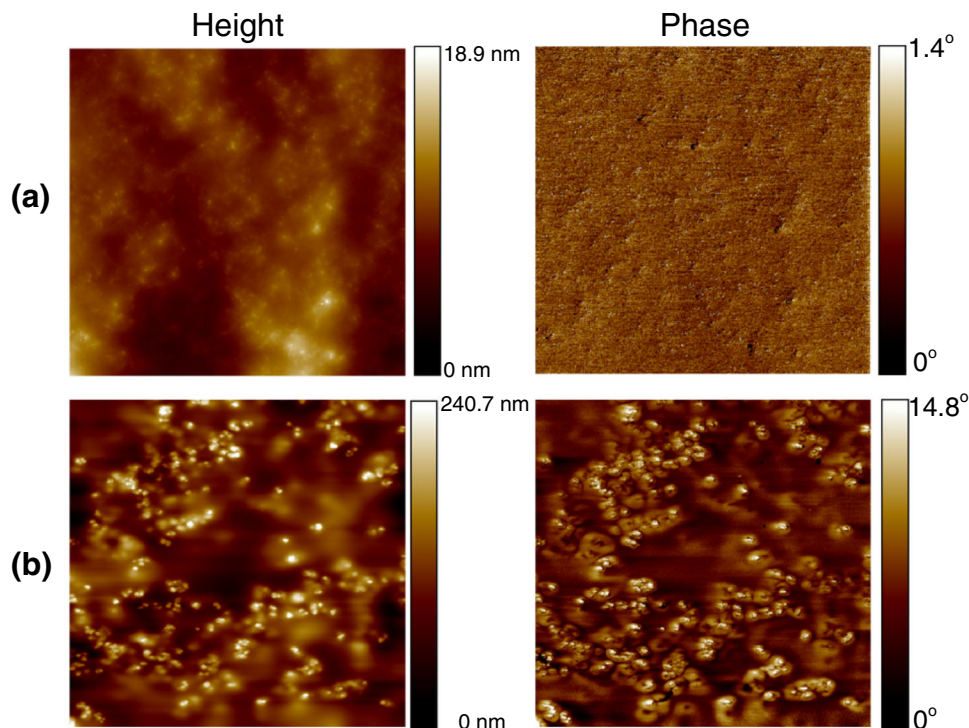


Fig. 1: AFM height images (left column) and phase images (right column) of nanocoating (a) unexposed and (b) exposed for 30 MJ/m² UV dose and at 40°C. Scan size is 20 μm \times 20 μm . The scale bars represent the height and phase range of each image

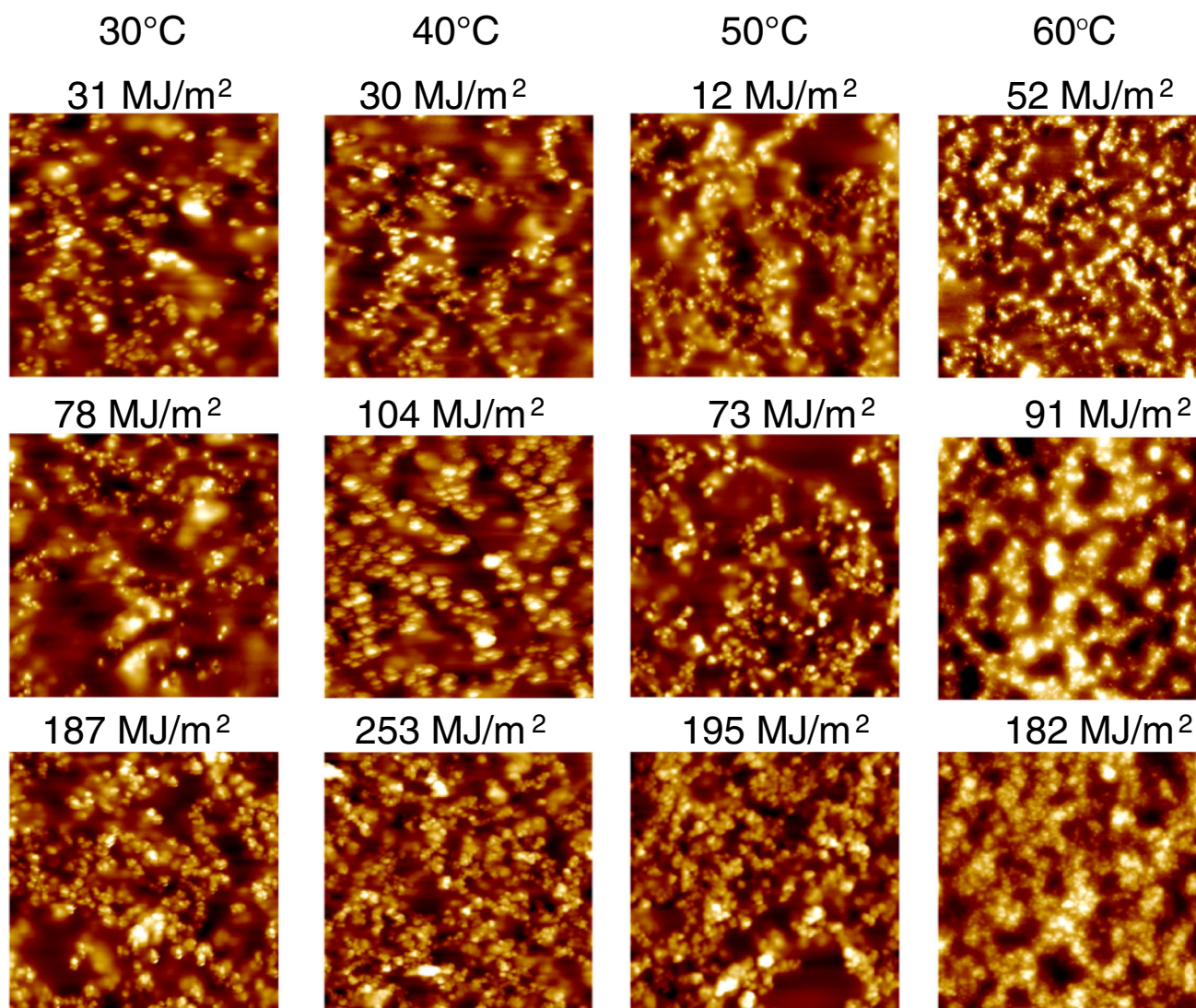


Fig. 2: AFM height images of epoxy nanocoating as a function of UV doses for four different temperatures; scan size: 20 μm × 20 μm. The height range of the images is roughly from 0 nm to 1.5 μm

silica nanoparticles that were embedded in the matrix were increasingly exposed on the surface. Figure 3 shows that a higher exposure temperature resulted in a higher amount of surface accumulation of nanosilica for dose less than 600 MJ/m². For example, at an exposure dose of 400 MJ/m², the surface coverages were approximately 45%, 50%, 56%, and 60% for 30, 40, 50, and 60°C, respectively. However, at doses of 700 MJ/m² or greater, there was essentially no difference in surface coverage between 50 and 60°C.

Chemical degradation

ATR-FTIR spectroscopy was used to follow chemical degradation of both neat epoxy (EP) and an amine-cured nanocoating (EP/SiO₂) as a function of UV dose

(or exposure times). For example, ATR-FTIR spectra of neat EP and EP/SiO₂ at 0 MJ/m², 60 MJ/m² (4 d), and 343 MJ/m² (23 d) at 40°C and 0% RH exposure conditions are shown in Fig. 4. Note that these spectra were obtained after normalizing to a reference band (1380 cm⁻¹, due to the gem-dimethyl CH₃) to account for any effect due to sampling. The selection of this reference band was because the intensity of this 1380 cm⁻¹ band showed little change up to the 340 MJ/m² dose through a parallel quantitative transmission FTIR study.²³ The assignment of the IR bands and detailed description can be found in references (20–23). Except for the 1000–1150 cm⁻¹ region, the spectral changes between the neat epoxy and the nanocoating are similar. In this region (1000–1150 cm⁻¹), the intensity increased for the nanocoating but decreased for the neat EP. This result was reflected

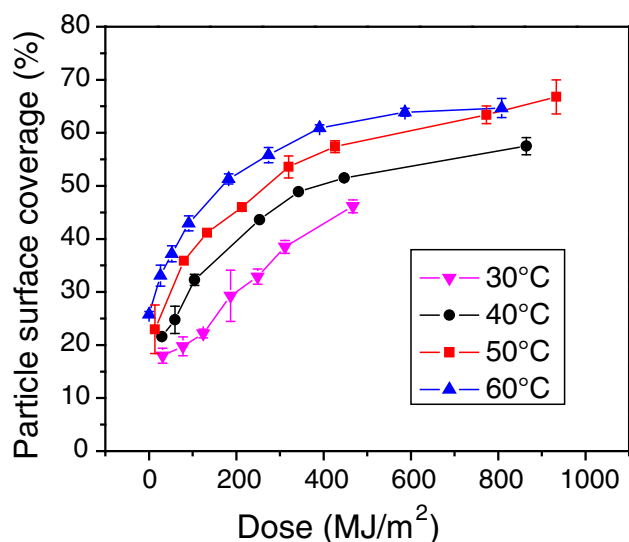


Fig. 3: Nanosilica coverage on epoxy nanocoating surface as a function of UV dose at four different temperatures as indicated in the legend. The coverage percentages were estimated using AFM bearing analysis on the height images from Fig. 2. Each data point is the average of three measurements ($20\ \mu\text{m} \times 20\ \mu\text{m}$ scan area). The error bars represent one standard deviation

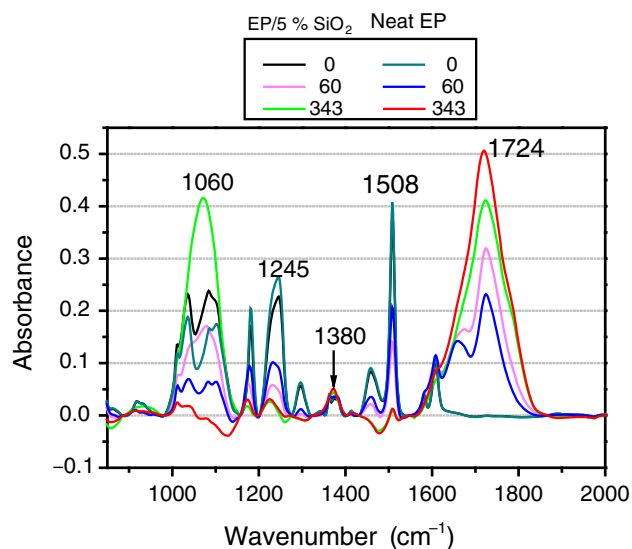


Fig. 4: ATR-FTIR spectra of neat epoxy (EP) and EP/5% SiO₂ nanocoating at three UV doses. The number corresponding to each colored line is the UV dose (MJ/m²). The band of interests is indicated in the graph

from a combination of band intensity related to Si–O–Si bonds (increased with UV dose) and various C–O bands decreased with UV dose. The band at $1060\ \text{cm}^{-1}$, which is attributed to epoxy C–O and Si–O bonds, was selected for monitoring surface accumulation of silica nanoparticles of nanocoating during UV exposure. Note that the intensity increase around

$1060\ \text{cm}^{-1}$ is actually an underestimate of the concentration of nanosilica detected.

The intensities of numerous bands of the epoxy structure substantially decreased under UV radiation, including the bands at $1508\ \text{cm}^{-1}$ due to the benzene ring, $1245\ \text{cm}^{-1}$ due to aromatic C–O. The decrease in the intensity of these bands, attributed to chain scission due to photodegradation, was observed in both neat EP and nanocoatings. New bands in the $1620\text{--}1740\ \text{cm}^{-1}$ region appeared and the intensities increased as UV dose increased. These bands were related to the photo-oxidation process. As shown in Fig. 4, the intensity at band $1724\ \text{cm}^{-1}$ increased faster in the neat EP than that of nanocoatings from 0 to $343\ \text{MJ/m}^2$ dose range. This result indicated that the addition of nanosilica reduced the rate of the photo-oxidation of the EP. Similar results were observed in the 60°C and 0% RH exposure conditions in our previous study.²³

The FTIR-ATR relative intensity changes (with respect to 0 d) at 1245 , 1724 , and $1060\ \text{cm}^{-1}$ bands after normalization to $1380\ \text{cm}^{-1}$ with UV dose are displayed in Fig. 5 for neat EP and EP/5%SiO₂ for four different temperatures. As discussed previously, the bands at 1245 and $1724\ \text{cm}^{-1}$, representing chain scission and oxidation of the epoxy, respectively, and at $1060\ \text{cm}^{-1}$, attributed to both epoxy C–O and Si–O bonds, were used to follow various degradation processes and surface accumulation of silica nanoparticles of nanocoating during UV exposure. The error bars in Fig. 5 show small standard deviations (except at high UV dose), indicating a good reproducibility between specimens. As shown in Figs. 5a and 5b for both EP and nanocoatings, the intensity of the bands at 1245 and $1724\ \text{cm}^{-1}$ changed rapidly at shorter/lower exposure time/dose ($<200\ \text{MJ/m}^2$), but reached a plateau value for dose $>400\ \text{MJ/m}^2$. The 60°C data show the highest degradation rate (fewer data points than other temperatures because of rapid degradation) among the four temperatures. Furthermore, the total changes in peak intensity at $1245\ \text{cm}^{-1}$ (Fig. 5a) and $1724\ \text{cm}^{-1}$ (Fig. 5b) were lower in nanocoatings than that in neat EP. This result indicated that the addition of nanosilica reduced the rate of the photo-oxidation of the EP, as mentioned earlier. However, there is no strong temperature effect on the rates of degradation in the dose range less than $200\ \text{MJ/m}^2$, except the 60°C data.

The intensity of the band at $1060\ \text{cm}^{-1}$ decreased in neat EP (Fig. 5c, left column) while it increased in nanocoatings (Fig. 5c, right column) with increasing UV dose, suggesting that silica has gradually accumulated on the specimen surface. This observation was confirmed by XPS measurements and our parallel particle release study using silane-treated nanosilica/EP coatings.²⁷ There is no clear trend in the temperature effect on this combined C–O and Si–O band. This is probably a result of two oppositely competing processes taking place on the nanocomposite surface during UV irradiation: loss of epoxy material (C–O

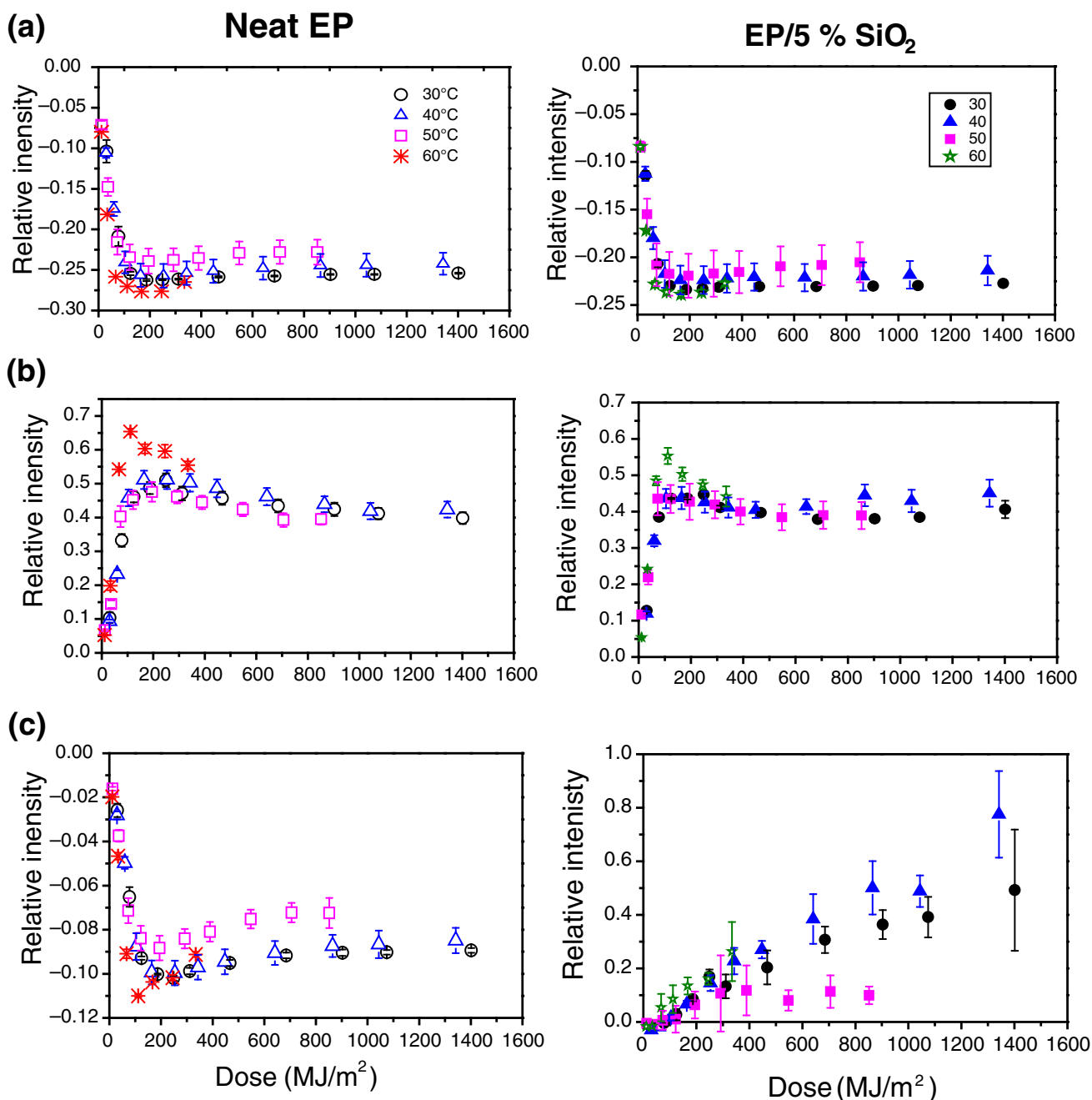


Fig. 5: ATR-FTIR relative intensity changes with UV dose at four temperatures for bands at: (a) 1245 cm⁻¹, (b) 1724 cm⁻¹, and (c) 1060 cm⁻¹ for neat EP (left column) and EP/5% SiO₂ (right column). The intensities have been normalized to that of the band at 1380 cm⁻¹. The results are average of 6 specimens, and error bars represent one standard deviation

loss, shown in Fig. 5c, left column) and increase of silica nanoparticles on the surface (Si–O increase).

In addition to FTIR data, UV-Vis measurements were also carried out on thinner nanocoating specimens (a 7 μm film on a CaF₂ substrate) to obtain the chemical degradation rate at various exposure temperatures. Figure 6 displays the chemical changes via UV-Vis absorbance at wavelength (λ) = 354 nm for both neat epoxy and nanocoatings at four different exposure

temperatures. In both materials, the absorbance increased as UV dose increased, and higher temperature had a higher rate of increase.

To detect the chemical composition on the nanocoating surface, XPS measurements were performed on the same samples after AFM measurements. Figure 7 displays the XPS-based carbon (C), oxygen (O), nitrogen (N), and silicon atomic (Si) percentages on the epoxy/nanosilica coating surface vs

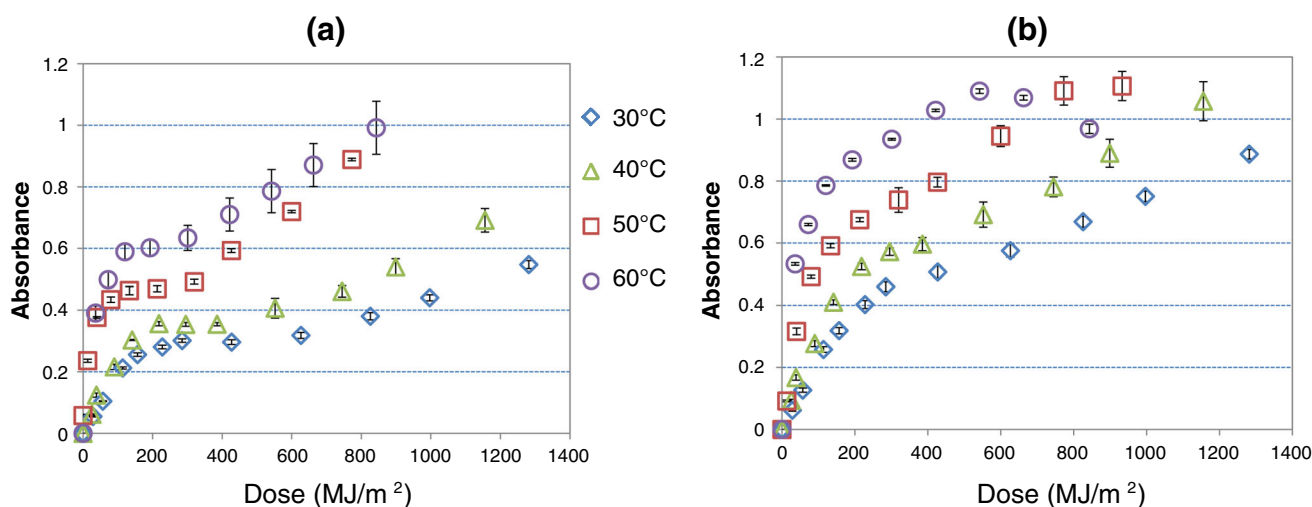


Fig. 6: UV–visible intensity at $\lambda = 354$ nm as a function of UV dose for (a) neat epoxy and (b) nanocoating for four different temperatures. The results are average of four specimens, and error bars represent one standard deviation. All absorbance values presented here are subtraction from values at exposure time = 0

UV dose. The loss of the epoxy matrix and an increase of the silica material near the nanocoating surface as a function of UV dose observed by ATR-FTIR in Figs. 5a (right column) and 5c (right column) are consistent with the XPS results displayed in Fig. 7. As the UV dose increased from 0 to 770 MJ/m² (≈ 60 d) at 60°C exposure condition, the percent surface concentrations of carbon decreased from $77.4 \pm 1.4\%$ to $50.2 \pm 1.7\%$, while those of silicon started at $3.4 \pm 0.8\%$, dropped after a small dose of 54 MJ/m² to $0.9 \pm 0.1\%$ followed by a steady rise to a final value of $6.5 \pm 0.4\%$, and nitrogen increased from $1.4 \pm 0.2\%$ to $8.1 \pm 0.2\%$. The increase of nitrogen with UV dose observed in Fig. 7 for nanosilica composite may be explained as due to the adsorption of the base amine curing agent on the acidic nanosilica surface during mixing and film formation. In this case, the adsorbed amine would form an interfacial layer between the silica nanoparticles and the epoxy polymer. Discussion on the formation of this interfacial layer is described in reference (23).

To get a better comparison visually, the increase of Si element percentage at different temperatures was plotted vs UV dose for four different temperatures; the results are displayed in Fig. 8. For doses less than 200 MJ/m², all data scattered around 2% with large error bars for all temperatures. Except for the 50°C exposure condition, the data do not follow a steady increase with temperature, and the last data point drops unexpectedly. In general, a higher exposure temperature resulted in a higher amount of Si element percentage for doses >200 MJ/m². However, the Si(2p) percentages increased with UV dose at a rate that increased with temperature. Extrapolated based on a linear fit of measurements (dose > 0 MJ/m²) at each temperature (not shown), the Si percentage that is at the surface for 600 MJ/m² is $2.5 \pm 0.1\%$, $2.8 \pm 0.2\%$,

$3.6 \pm 0.3\%$, and $5.4 \pm 0.4\%$ for 30, 40, 50, and 60°C, respectively. This result is in agreement with temperature effects on nanosilica surface accumulation data obtained by AFM measurements shown in Fig. 3. Note that the Si element percentage at 0 dose is about (2–3) %, which is much smaller than the initial offset particle surface coverage estimated from AFM measurements (Fig. 3). The reason is due to different detection mechanisms and limitations between two techniques. AFM image estimation is based on particles raised above the surface, which include those covered with a thin layer of the matrix. AFM can scan the surface with height variation as large as a few microns (up to 1.5 μm in Fig. 2). As mentioned previously, because of the complication in the surface morphology of nanocoatings (e.g., rough surface and some silica particles were embedded in EP matrix or formed a larger cluster size), the percent of particle surface coverage can be overestimated. On the other hand, XPS data are based on mostly bare Si material and the probing depth is only a few nm. Even multiplying a factor of 60/28 (molecular mass of SiO₂/molecular mass of Si assuming that all Si were from SiO₂), the percentage is still lower than 10%. Therefore, the amounts of nanosilica estimated by AFM are expected to be greater than those measured by XPS.

Kinetics analysis

To examine the temperature effects on photodegradation and nanosilica surface accumulation, UV dose-dependent curves of particle surface coverage via AFM (Fig. 3) and UV–Vis absorbance @340 nm (Fig. 6—both EP and EP-5% SiO₂) were fitted to an exponential function equation (1), and Si elemental percentage via XPS (Fig. 8) to a linear relationship equation (2).

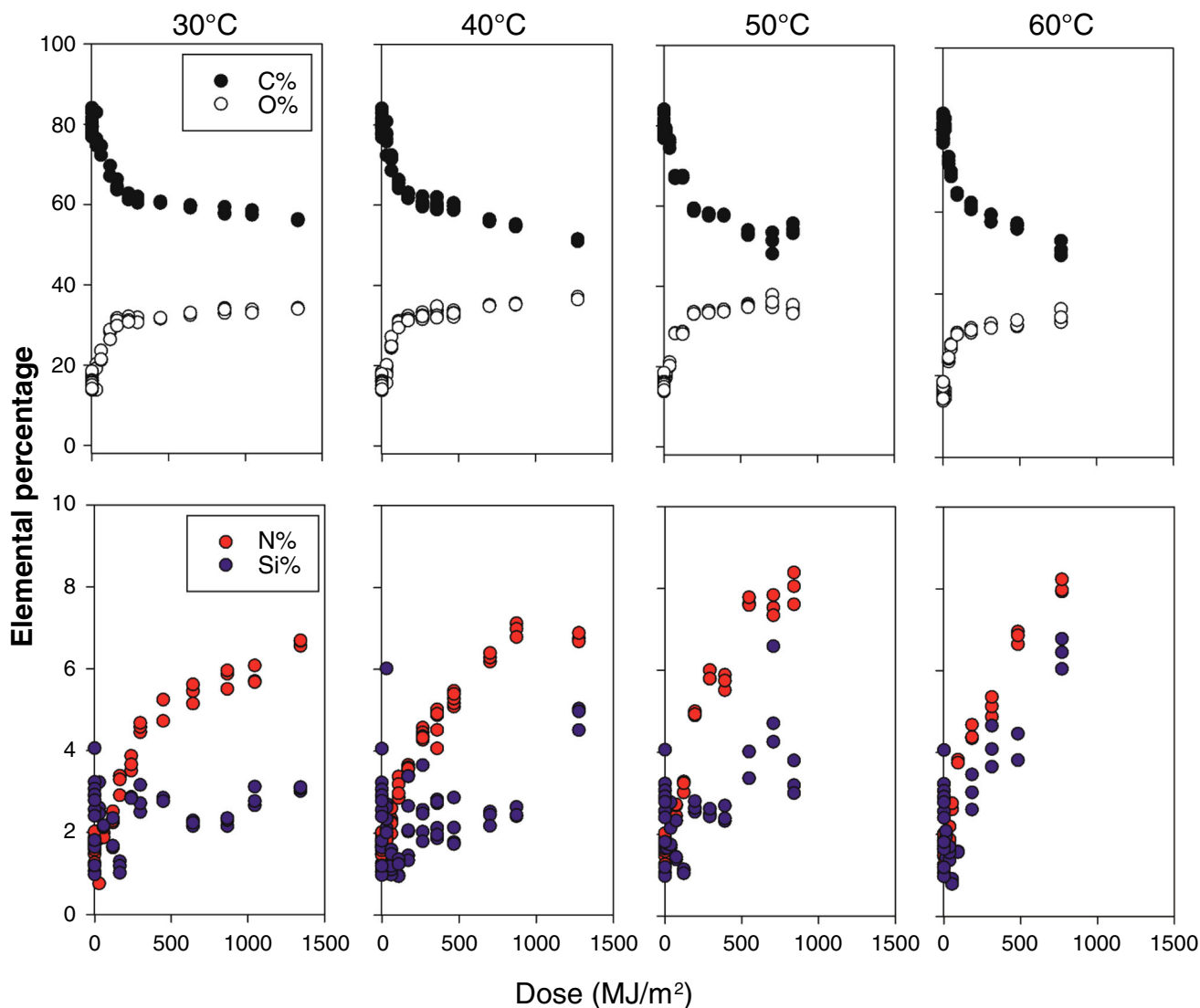


Fig. 7: XPS-based carbon, nitrogen, and silicon atomic percentages on the epoxy/nanosilica coatings surface vs UV irradiation dose (MJ/m²). At the same dose (exposure time), more than two locations were measured as shown in the graphs

$$I(\tau) = A * \exp(-k * \tau) + I_0 \tag{1}$$

$$I(\tau) = k * \tau + I_0 \tag{2}$$

where $I(\tau)$ is the relative change of degradation property (or damage) at dose = τ , I_0 is intercept at dose (τ) = 0, and k is the rate of change per UV dose (MJ/m²). The fitted kinetic parameters are listed in Table 1. The goodness (R^2 , not listed here) of fitting for UV-Vis and AFM data is good arranging from 0.95 to 0.99, but only 0.20, 0.72, 0.80, and 0.82 for XPS data @ 30, 40, 50, and 60°C, respectively, due to larger error bars in Fig. 8. The degradation rates (k) determined from UV-Vis absorbance @340 nm data for EP are higher than those of nanocoatings for all temperatures. This result implies that nanosilica additives induce the

delay in the photodegradation process, which is consistent with the results observed through FTIR results. However, there are no kinetic parameters extracted from ATR-FTIR data. Based on the observations in Figs. 5a and 5b (1245, 1724 cm⁻¹), temperature had little effect on the rates of degradation in the dose range less than 200 MJ/m², except the 60°C data. Note that these IR bands were normalized by peak intensity at band 1380 cm⁻¹. And there is no clear trend in the temperature effect on intensity changes at band 1245 cm⁻¹. Moreover, the peak intensity at the reference band (1380 cm⁻¹) started to decrease around 300 MJ/m² UV dose or higher due to increase in specimen surface roughness (especially, for the EP-5% SiO₂ coatings). The ATR-FTIR data beyond this dose were not reliable; thus, the estimated kinetic parameters were not reliable extracted from the ATR-FTIR data.

The reaction rates are expected to increase with temperature according to Arrhenius equation (3).²⁸

$$k = A_e * \exp(-E_a/T) \tag{3}$$

where k is the rate of reaction, A_e is the pre-exponential factor, E_a is the activation energy, R is the gas constant, and T is the absolute temperature in Kelvin ($^{\circ}\text{K} = 273.12 + ^{\circ}\text{C}$). As shown in Table 1, the rates for all degradation properties increase with

increasing temperature. The activation energy can be determined by plotting the natural logarithm of the relative rates against $1/T(^{\circ}\text{K})$, and the results are listed in Table 1. Overall, the activation energy (kJ/mol) determined from UV-Vis results is reasonable; the difference in EP and EP/SiO₂ is insignificant. The activation energy determined from XPS method is much higher than that from AFM. Further investigation on the correlation between the values of activation energy and degradation mechanism via detection methods is ongoing.

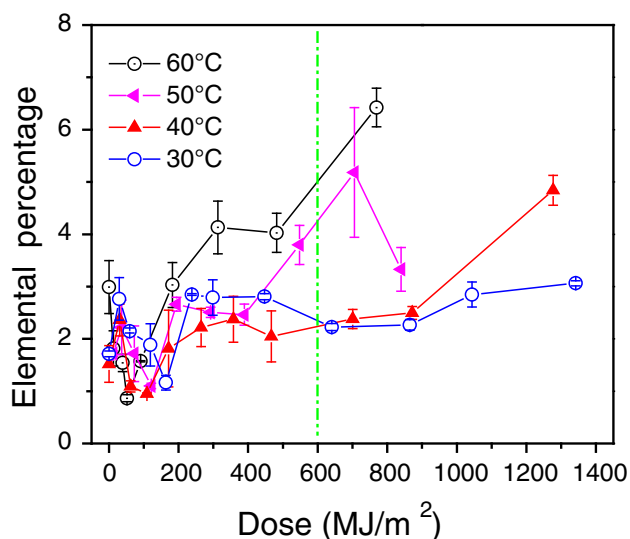


Fig. 8: XPS-based silicon (Si) % elemental percentage on the epoxy/nanosilica coatings surface vs UV irradiation dose at four different temperatures. Each data point consists of two or more specimens, and the error bars represent one standard deviation. The dashed line indicates the dose at 600 MJ/m²

Concluding remarks

The effects of temperature on both the photodegradation of epoxy matrix and surface accumulation of nanosilica during UV exposures of an epoxy coating containing 5 mass% nanosilica were investigated through a suite of techniques, such as FTIR, XPS, UV-Vis, and AFM. The FTIR and UV-Vis results indicated that the addition of nanosilica reduces the rate of the photodegradation of the EP. For the effect of temperature on the degradation rate, all results (except FTIR data) indicated that the higher temperature, the higher photodegradation and surface nanosilica accumulation rate. The chemical degradation rate of the matrix (UV-Vis data in Fig. 6) and accumulation rate for Si on the surface (via AFM: Fig. 3 and via XPS data in Fig. 8) followed the right temperature order, i.e., 60°C > 50°C > 40°C > 30°C. The corresponding degradation kinetic parameters and activation energy were also obtained, and the rates for all degradation properties increase with increasing temperature, as expected (Arrhenius relationship). These kinetic parameters are useful for understanding

Table 1: Kinetics parameters (I_0 , A , k) and activation energy (E_a) for three different degradation properties for EP and EP/SiO₂ coatings at four different temperatures

Degradation property	Kinetic parameter	30°C	40°C	50°C	60°C	Activation energy E_a (kJ/mol)
UV-Vis absorption @ $\lambda = 354$ nm	I_0	0.316 ± 0.015	0.389 ± 0.022	0.462 ± 0.007	0.603 ± 0.015	32.12 ± 8.63
	A	-0.239 ± 0.017	-0.399 ± 0.022	-0.400 ± 0.011	-0.600 ± 0.023	
EP (Fig. 6a)	k	0.009 ± 0.001	0.010 ± 0.002	0.040 ± 0.003	0.027 ± 0.003	38.92 ± 3.27
UV-Vis @ $\lambda = 354$ nm	I_0	0.596 ± 0.015	0.652 ± 0.025	0.765 ± 0.021	0.895 ± 0.038	
EP/5%SiO ₂ (Fig. 6b)	A	-0.607 ± 0.015	-0.656 ± 0.024	-0.766 ± 0.028	-0.879 ± 0.059	18.59 ± 4.60
	k	0.005 ± 0.001	0.007 ± 0.001	0.012 ± 0.001	0.020 ± 0.003	
Surface particle coverage via AFM	I_0	60.68 ± 7.67	58.42 ± 0.99	65.59 ± 0.99	64.85 ± 0.68	64.48 ± 11.21
	A	-54.56 ± 4.84	-42.02 ± 1.03	-44.45 ± 1.73	-37.93 ± 0.81	
EP/5%SiO ₂ (Fig. 3)	k	0.0028 ± 0.0008	0.0042 ± 0.0003	0.0039 ± 0.0004	0.0057 ± 0.0004	
Si element via XPS	I_0	2.093 ± 0.218	1.509 ± 0.203	1.543 ± 0.239	2.187 ± 0.312	
EP/5%SiO ₂ (Fig. 8)	K	0.0007 ± 0.0003	0.0021 ± 0.0004	0.0049 ± 0.0005	0.0053 ± 0.0009	

A is the pre-exponential factor, I_0 is intercept at 0 dose, and k is the rate of change per UV dose (MJ/m²). E_a is the activation energy

the degradation mechanism and for predicting the service life of the exterior nanocoatings.

Disclaimer

Certain commercial product or equipment is described in this paper in order to specify adequately the experimental procedure. In no case does such identification imply recommendation or endorsement by the National Institute of Standards and Technology, nor does it imply that it is necessarily the best available for the purpose.

References

1. Wohlleben, W, Neubauer, N, “Quantitative Rates of Release from Weathered Nanocomposites are Determined Across 5 Orders of Magnitude by the Matrix, Modulated by the Embedded Nanomaterial.” *NanoImpact*, **1** 39–45 (2016)
2. Grand View Research. Global Nanocoatings Market, accessed on August 9, 2016 <https://www.grandviewresearch.com/press-release/global-nanocoatings-market> (2016)
3. Zhang, J, Terrones, M, Park, CR, Mukherjee, R, Monthioux, M, Koratkar, N, et al., “Carbon Science in 2016: Status, Challenges and Perspectives.” *Carbon*, **98** 708–732 (2016)
4. Liu, YY, Zhao, J, Zhao, LY, Li, WW, Zhang, H, Yu, X, et al., “High Performance Shape Memory Epoxy/Carbon Nanotube Nanocomposites.” *ACS Appl. Mater. Interfaces*, **8** (1) 311–320 (2016)
5. Shah, MSA, Nag, M, Kalagara, T, Singh, S, Manorama, SV, “Silver on PEG-PU-TiO₂ Polymer Nanocomposite Films: An Excellent System for Antibacterial Applications.” *Chem. Mater.*, **20** 2455–2460 (2008)
6. Nadiv, R, Shtein, M, Refaeli, M, Peled, A, Regev, O, “The Critical Role of Nanotube Shape in Cement Composites.” *Cem. Concr. Compos.*, **71** 166–174 (2016)
7. Nowack, B, David, RM, Fissan, H, Morris, H, Shatkin, JA, Stintz, M, Zepp, R, Brouwer, D, “Potential Release Scenarios for Carbon Nanotubes Used in Composites.” *Environ. Int.*, **59** 1–11 (2013)
8. Wohlleben, W, Vilar, G, Fernandez-Rosas, E, Gonzalez-Galvez, D, Gabriel, C, Hirth, S, et al., “A Pilot Interlaboratory Comparison of Protocols That Simulate Aging of Nanocomposites and Detect Released Fragments.” *Environ. Chem.*, **11** (4) 402–441 (2014)
9. Ducan, TV, “Release of Engineered Nanomaterials from Polymer Nanocomposites: The Effect of Matrix Degradation.” *ACS Appl. Mater. Interfaces*, **7** (1) 20–39 (2015)
10. Froggett, SJ, Clancy, SF, Boverhof, DR, Canady, RA, “A Review and Perspective of Existing Research on the Release of Nanomaterials from Solid Nanocomposites.” *Part. Fibre Toxicol.*, **11** (17) 1–28 (2014)
11. Fernández-Rosas, E, Vilar, G, Janer, G, González-Gálvez, D, Puentes, V, Jamier, V, et al., “Influence of Nanomaterials Compatibilization Strategies in Polyamide Nanocomposite Properties and Nanomaterials Release During the Use Phase.” *Environ. Sci. Technol.*, **50** (5) 2584–2594 (2016)
12. Nguyen, T, Wohlleben, W, Sung, LP, “Mechanisms of Aging and Release from Weathered Nanocomposites.” In: Wohlleben, W, Kuhlbusch, T, Schnekenburger J, Lehr, CM (eds.) *Safety of Nanomaterials along Their Lifecycle: Release, Exposure, and Human Hazards*, pp. 315–334. CRC Press, 2014
13. Gottschalk, F, Nowack, B, “The Release of Engineered Nanomaterials to the Environment.” *J. Environ. Monit.*, **13** (5) 1145–1155 (2011)
14. Wohlleben, W, Meyer, J, Muller, J, Muller, P, Vilsmeier, K, Stahlmecke, B, et al., “Release from Nanomaterials During Their Use Phase: Combined Mechanical and Chemical Stresses Applied to Simple and Multi-Filler Nanocomposites Mimicking Wear of Nano-Reinforced Tires.” *Environ. Sci. Nano*, **3** (5) 1036–1051 (2016)
15. Ging, J, Tejerina-Anton, R, Ramakrishnan, G, Murphy, K, Gorham, JM, et al., “Development of a Conceptual Framework for Evaluation of Nanomaterials Release from Nanocomposites: Environmental and Toxicological Implications.” *Sci. Total Environ.*, **473** 9–19 (2014)
16. Petersen, EJ, Diamond, SA, Kennedy, AJ, Goss, GG, Ho, K, Lead, J, et al., “Adapting OECD Aquatic Toxicity Tests for Use with Manufactured Nanomaterials: Key Issues and Consensus Recommendations.” *Environ. Sci. Technol.*, **49** (16) 9532–9547 (2015)
17. Godwin, H, Nameth, C, Avery, D, Bergeson, LL, Bernard, D, Beryt, E, et al., “Nanomaterial Categorization for Assessing Risk Potential to Facilitate Regulatory Decision-Making.” *ACS Nano*, **9** (4) 3409–3417 (2015)
18. Selck, H, Handy, RD, Fernandes, TF, Klaine, SJ, Petersen, EJ, “Nanomaterials in the Aquatic Environment: A European Union-United States Perspective on the Status of Ecotoxicity Testing, Research Priorities, and Challenges Ahead.” *Environ. Toxicol. Chem.*, **35** (5) 1055–1067 (2016)
19. Chin, J, Byrd, E, Embree, E, et al., “Accelerated UV Weathering Device Based on Integrating Sphere Technology.” *Rev. Sci. Instrum.*, **75** 4951–4959 (2004)
20. Nguyen, T, Pellegrin, B, Bernard, C, Gu, X, Gorham, JM, Stutzman, P, Stanley, D, Shapiro, A, Byrd, E, Hettenhouser, R, Chin, J, “Fate of Nanoparticles During Life Cycle of Polymer Nanocomposites.” *J. Phys. Conf. Ser.*, **304** 012060 (2011)
21. Gorham, JM, Nguyen, T, Bernard, C, Stanley, D, Holbrook, RD, “Photo-Induced Surface Transformations of Silica Nanocomposites.” *Surf. Interface Anal.*, **44** 1572–1581 (2012)
22. Nguyen, T, Pellegrin, B, Bernard, C, Rabb, S, Stutzman, P, Gorham, JM, Gu, X, Yu, LL, Chin, J, “Characterization of Surface Accumulation and Release of Nanosilica During Irradiation of Polymer Nanocomposites by Ultraviolet Light.” *J. Nanosci. Nanotechnol.*, **12** 6202–6215 (2012)
23. Sung, L, Stanley, D, Gorham, JM, Rabb, SA, Gu, X, Yu, LL, Nguyen, T, “Characterization of Surface Accumulation and Release of Nanosilica During Irradiation of Polymer Nanocomposites by Ultraviolet Light.” *J. Coat. Technol. Res.*, **12** (1) 121–135 (2015)
24. Jacobs, D, Huang, SR, Cheng, YL, Rabb, S, Gorham, JM, Krommenhoek, PJ, Yu, LL, Nguyen, T, Sung, L, “Investigating the Process of Surface Degradation and Nanoparticle Release of a Commercial Nanosilica/Polyurethane Coating Under UV Exposure.” *J. Coat. Technol. Res.*, **13** (5) 735–751 (2016)
25. Robinson, J, Linder, A, Gemmel, A, Poulsen, KV, Burkhard, H, Högström, P, et al., “In Comparison of Standard UV Test Methods for the Ageing of Cables.” *60th IWCS Conference*, Charlotte, NC, 2011
26. Pickett, JE, Gardner, MM, Gilbson, DA, Rice, ST, “Goal Weathering of Aromatic Engineering Thermoplastics.” *Polym. Degrad. Stab.*, **90** 405–415 (2005)
27. Tien, CC, Chang, CH, Liu, B, Stanley, D, Rabb, SA, Yu, LL, Nguyen, T, Sung, L, “Effects of Temperature on Surface Accumulation and Release of Silica Nanoparticles in an Epoxy Nanocoating Exposed to UV Radiation.” *Nanotech Proceeding*, Washington DC, June 2014
28. Pickett, JE, Gilbson, DA, Rice, ST, Gardner, MM, “Effects of Temperature on the Weathering of Engineering Thermoplastics.” *Polym. Degrad. Stab.*, **93** 684–691 (2006)